Dalton Transactions

PAPER

View Article Online
View Journal | View Issue

Cite this: *Dalton Trans.*, 2016, **45**, 18622

Solvent-induced structural diversity in tetranuclear Ni(II) Schiff-base complexes: the first Ni_4 single-molecule magnet with a defective dicubane-like topology†

Radovan Herchel, Ivan Nemec, Marek Machata and Zdeněk Trávníček*

Two tetranuclear Ni^{II} complexes, namely $[Ni_4(L)_4(CH_3OH)_3(H_2O)]\cdot CH_3OH$ (**1**) and $(Pr_3NH)_2[Ni_4(L)_4(CH_3COO)_2]$ (**2**, Pr_3N = tripropylamine), were synthesized from a tridentate Schiff base ligand H_2L (2-[(*E*)-(2-hydroxybenzylidene)amino]phenol) and $Ni(CH_3COO)_2\cdot 4H_2O$, using different solvents and their ratios (CH_3OH and/or CH_2Cl_2). The prepared Ni_4 complexes are of different structural types, involving an Ni_4O_4 cubane-like core (**1**) and Ni_4O_6 defective dicubane-like core (**2**), with all the Ni atoms hexacoordinated. The complexes were characterized by elemental analysis, FT-IR spectroscopy, variable temperature and field magnetic measurements, and single crystal X-ray analysis. The DFT and CASSCF/NEVPT2 theoretical calculations were utilized to reveal information about the isotropic exchange parameters (J_{ij}) and single-ion zero-field splitting parameters (D_i, E_i). The variable temperature magnetic data suggested the competition of the antiferromagnetic and ferromagnetic intracluster interactions in compound **1**, which is in contrast to compound **2**, where all intracluster interactions are ferromagnetic resulting in the ground spin state $S = 4$ with an easy-axis type of anisotropy quantified by the axial zero-field splitting parameter $D = -0.81\ cm^{-1}$. This resulted in the observation of a field-induced slow-relaxation of magnetization (U = 3.3–6.7 K), which means that the complex **2** represents the first Ni_4 single-molecule magnet with the defective dicubane-like topology.

Received 9th September 2016,
Accepted 19th October 2016

DOI: 10.1039/c6dt03520e

www.rsc.org/dalton

Introduction

Polynuclear coordination compounds with paramagnetic metal centers have attracted much attention over the last few decades due to their potential application as a new type of magnetic material. Such molecular compounds may exhibit slow-relaxation of magnetization of the molecular origin and thus they can behave as single-molecule magnets (SMMs).[1] Interesting quantum phenomena such as quantum tunneling of magnetization (QTM),[1b] quantum coherence[1g] and quantum interference[1i] have been found in such compounds. SMMs have the potential to be utilized in ultra-high density data storage devices,[1a,j] quantum computing[1c] or molecular spintronics.[1h] Despite the recent achievements in the research of SMMs with one paramagnetic metal center (so called single-ion magnets),[2] in order to obtain SMMs, the synthesis of high-spin polynuclear metal complexes is the most used approach at all.[3] For obtaining such compounds it is essential to modulate molecular properties so that the coupling between neighboring metal centers results in the non-zero ground spin state with $S > 1/2$, and most importantly, the metal centers should have non-negligible magnetic anisotropy.

In designing SMMs, coordination compounds involving Ni^{II} metal centers are particularly attractive because they can possess large magnetic anisotropy on their central atoms.[4] Furthermore, it is of interest that multiple polynuclear Ni^{II} compounds have often been shown to exhibit slow-relaxation of magnetization.[5,6] Among such polynuclear Ni^{II} complexes, compounds belonging to the class containing a tetranuclear Ni–O–Ni bridged cubane-like core have been intensively studied for the last few decades.[6k,7–11] For this type of compound a correlation between the sign and value of the magnetic exchange constant (J) and structural properties has been established.[8] According to these studies the Ni–O–Ni angle has been recognized as the most important parameter.[8a] The magnetic exchange is expected to be ferromagnetic, when the bond angle is close to 90°, while as the Ni–O–Ni angle increases, the value of J decreases following a linear relationship. When the

Department of Inorganic Chemistry, Regional Centre of Advanced Technologies and Materials, Faculty of Science, Palacký University, 17. listopadu 12, CZ-771 46 Olomouc, Czech Republic. E-mail: zdenek.travnicek@upol.cz

†Electronic supplementary information (ESI) available: Additional X-ray data, magnetic data and analysis, and details of theoretical calculations. CCDC 1443519–1443520. For ESI and crystallographic data in CIF or other electronic format see DOI: 10.1039/c6dt03520e

angle is close to 99° the magnetic coupling between the Ni^{II} atoms becomes antiferromagnetic. In some of the cases, the absolute value of $|J|$ can exceed 20 cm^{-1}.[7] However, some examples can be found which do not follow the above-mentioned relationship.[12,17b] This can be explained by additional structural factors influencing exchange interactions such as the Ni–O bond distance, the dihedral angle within the Ni_2O_2 unit and the Ni–O–R angle (R = substituent covalently bound to the bridging oxygen atom) or the presence of an additional bridging group which may also affect the character and strength of the exchange coupling.[11,17b]

While numerous studies have recently investigated cubane-like Ni^{II} complexes,[5f,8,9,10] which in some cases showed slow-relaxation of magnetization,[5] only a few studies have focused on Ni^{II} complexes with a defective dicubane-like Ni_4O_6 core with one shared face and one vertex missing from each cube (Fig. 1).[8e,13] Interestingly, both mentioned types of Ni^{II} complexes can be advantageously obtained by the reaction of a Ni^{II} salt and polydentate ligands such as Schiff bases, in which oxygen atoms of phenoxo, alkoxo or hydroxo groups can act as μ^2 or μ^3 bridging atoms incorporated in the cubane/defective dicubane core.[5d,8d,e,10] Furthermore, minor ligand changes can significantly affect the Ni–O–Ni bond angles and Ni···Ni distances across the faces of the distorted cube significantly and thus, they can change the magnetic properties of the prepared complexes considerably.[8c,16d] In this context, polydentate Schiff base ligands derived from salicylaldehyde and its derivatives are good candidates to be used for the synthesis of novel cubane-like Ni^{II} complexes,[14,15b,17d] and also, for the study of not so well explored defective dicubane-like Ni^{II} complexes.[13c,d] The assembly process is also dependent upon the crystallization conditions, such as temperature, solvent, pH and concentration of reagents.[8c,e,13c,d] All these factors can also significantly influence both the structure and magnetic properties of the resulting compounds. For example, Meyer and co-workers showed how the incorporation of different solvent molecules in the coordination sphere of Ni^{II} atoms within a distorted cubane core resulted in the switching paramagnetic S = 4 ground state into the diamagnetic S = 0 ground state.[8c]

Herein, we report the preparation, structural and magnetic properties of two tetranuclear Ni^{II} complexes with different topologies depending on different preparation conditions (solvents' ratio, Fig. 1): a cubane-like complex $[Ni_4(L)_4(CH_3OH)_3(H_2O)]$ (**1**, CH_2Cl_2 : CH_3OH = 3 : 1) and a defective dicubane-like complex $(Pr_3NH)_2[Ni_4(L)_4(CH_3COO)_2]$ (**2**, Pr_3NH^+ = tripropylammonium cation, CH_2Cl_2 only). As a ligand the Schiff base H_2L (2-[(*E*)-(2-hydroxybenzylidene)amino]phenol) with the $\{NO_2\}$ donor set was used.

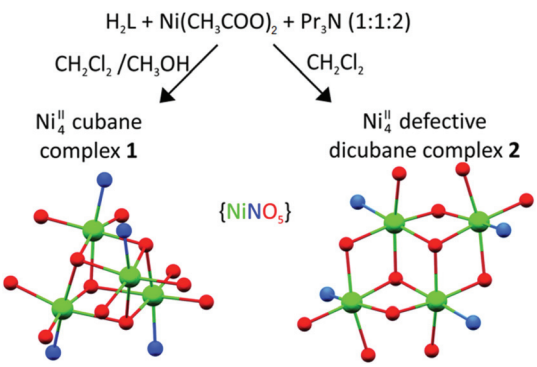

Fig. 1 The scheme describing the preparation of compounds **1–2**.

Results and discussion

Synthesis

Two different tetranuclear Ni_4 complexes were successfully synthesized by the reaction of a tridentate Schiff base ligand H_2L and $Ni(CH_3COO)_2{\cdot}4H_2O$ in the molar ratio of 1 : 1 in the presence of Pr_3N as a base using distinct reaction media (Fig. 1): a cubane complex **1** (CH_3OH–CH_2Cl_2 in the volume ratio 1 : 3) and a defective dicubane complex **2** (CH_2Cl_2 only). The fact that the reactions in different solvents resulted in the formation of different complexes can be reasonably explained on the basis of their crystal structures. In particular, the way how the solvent molecule is involved (or not involved) in the molecular structure of each compound affects the resulting composition significantly (*vide infra*).

Description of structures

General features. The utilized ligand H_2L (and its derivatives) coordinates usually metal atoms in a tridentate manner (the NO_2 atom donor set) by one imine nitrogen atom (N_{Im}) and two phenolate oxygen atoms which can act also as bridging atoms (Fig. 2).[8e,15]

The ligands are asymmetric and can be divided into the salicylaldehydic and aminophenolic parts respective to the reactants they originate from. The ligand asymmetry is apparent when inspecting the bridging function of the oxygen atoms. For example, previously reported Fe^{III} complexes involve both types of the oxygen atoms in their structure (O_{Sal} in the salicylaldehydic part, O_A in the aminophenolic part) as donor atoms, but only the O_A atoms serve as the bridging ones.[15a–g] However, the further examples involving Ni^{II}_4,[15k] $Ni^{II}_2Ln^{III}_2$[15h] and $Fe^{III}_2Ln^{III}$ (ref. 15*i*,*m*) complexes (where Ln = Gd, Tb, Dy) with L^{2-} or 3m-L^{2-} ligands (H_2-3m-L = (2-[(*E*)-(2-hydroxy-3-methoxy-benzylidene)amino]phenol)) possessed the O_{Sal} atoms also in a bridging function. In both compounds (**1–2**),

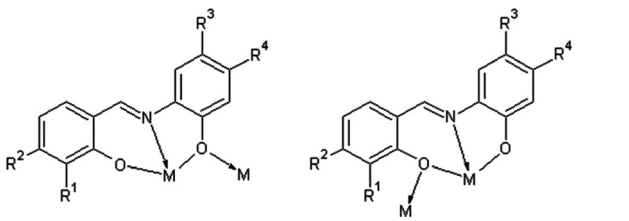

Fig. 2 Schematic representations of the binding abilities of the ligand H_2L and its derivatives.

the complex moieties contain four Ni^{II} atoms and four doubly deprotonated Schiff base ligands L^{2-}. Basic differences between the crystal structures of **1** and **2** can be summarized into several points. Firstly, a cubane-like core can be found in **1**, whereas compound **2** contains a defective dicubane core. Secondly, despite the same reactants used in the preparation of **1** and **2** their composition differs significantly. In **1**, methanol molecules are incorporated both into the complex molecule as ligands and into the crystal structure as lattice solvent molecules, with important consequences for crystal packing (*vide infra*). In **2**, two CH_3COO^- anions are incorporated in the molecular structure. Finally, it can be seen that the metal centers in both **1** and **2** are hexacoordinated with the $\{NiNO_5\}$ chromophores (Fig. 1 and 3).

$[Ni_4(L)_4(CH_3OH)_3(H_2O)]\cdot CH_3OH$ (1). Complex **1** crystallizes in the triclinic space group $P\bar{1}$ (Table S1†). The asymmetric unit comprises one electroneutral tetranuclear $[Ni_4(L)_4(CH_3OH)_3(H_2O)]$ molecule (Fig. 3a) and one lattice CH_3OH molecule. The $[Ni_4(\mu^3\text{-}O_A)_4]$ cubane core (Fig. 3b) consists of the O_A atoms of the Schiff base ligand and the Ni^{II} atoms occupying the alternating vertices of the distorted cube, similarly to other Schiff base Ni^{II} cubane-like core compounds.[8d,e,16,17] Each hexacoordinated Ni^{II} atom in the complex molecule of **1** involves the same coordination environment with similar bond lengths. The axial positions in the coordination polyhedron are occupied by the oxygen atoms from the coordinated solvent molecules (O_{Solv}) and by the μ^3-O_A atoms from the adjacent L^{2-} ligands.

In three cases, the O_{Solv} atoms originate from the CH_3OH molecules (d(Ni–O_{Solv}) = from 2.10 to 2.11 Å) and in one case from H_2O molecules (d(Ni–O_{Solv}) = 2.085(3) Å). The axial Ni–O_A bonds are the longest with bond distances ranging from 2.22 to 2.28 Å. Each Ni atom in **1** has the equatorial positions occupied by three donor atoms from chelating ligand L^{2-} (μ^3-O_A, O_{Sal} and N_{Im} atoms) and the fourth position is occupied by the μ^3-O_A atom from the adjacent L^{2-} ligand. The Ni–N_{Im} bonds adopt the shortest lengths: d(Ni–N_{Im}) = 1.97–1.98 Å. The Ni–O_A bonds within the chelate ring of the L^{2-} ligand are significantly longer (from 2.04 to 2.07 Å) than the Ni–O_{Sal} bonds (from 1.95 to 1.97 Å).

The coordinated solvent molecules are involved in the stabilization of the cubane core as it was observed previously in other cubane-based Ni^{II} compounds.[5d,8a,c,e,16,18] The hydrogen bonds between the solvent molecules (CH_3OH, H_2O as hydrogen

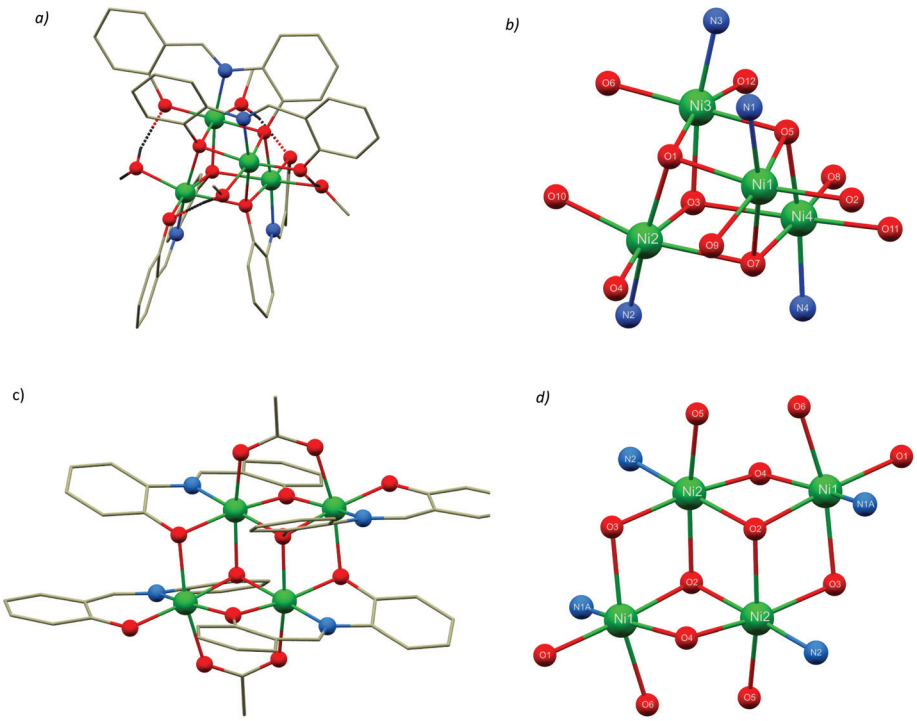

Fig. 3 Molecular structure of the complex molecule in **1** (a) and view on a cubane-like core of **1** (b). Hydrogen atoms were omitted for clarity, except for those which are involved in intramolecular hydrogen bonding (O–H···O black dashed lines). Bond distances (in Å) within the coordination polyhedra: (Ni1–O1) = 2.052(2), (Ni1–O2) = 1.957(2), (Ni1–O5) = 2.234(2), (Ni1–O7) = 2.069(2), (Ni1–O9) = 2.111(2), (Ni1–N1) = 1.978(3), (Ni2–O1) = 2.037(2), (Ni2–O3) = 2.067(2), (Ni2–O4) = 1.955(2), (Ni2–O7) = 2.283(2), (Ni2–O10) = 2.085(3), (Ni2–N2) = 1.967(3), (Ni3–O1) = 2.248(2), (Ni3–O3) = 2.055(2), (Ni3–O5) = 2.049(2), (Ni3–O6) = 1.953(2), (Ni3–O12) = 2.111(2), (Ni3–N3) = 1.968(3), (Ni4–O3) = 2.221(2), (Ni4–O5) = 2.055(2), (Ni4–O7) = 2.044(2), (Ni4–O8) = 1.974(2), (Ni4–O11) = 2.097(2), (Ni4–N4) = 1.975(3). Molecular structures of the complex anion in **2** (c) and view on a defective dicubane core of **2** (b). Bond distances (in Å) within the coordination polyhedra for **2**: (Ni1–O1) = 2.0076(19), (Ni1–O2A) = 2.0474(17), (Ni1–O3) = 2.1810(16), (Ni1–O4) = 2.0387(16), (Ni1–O6) = 2.1050(16), (Ni1–N1) = 2.030(5), (Ni2–O2) = 2.1396(15), (Ni2–O2A) = 2.0549(16), (Ni2–O3) = 2.0580(17), (Ni2–O4) = 2.9994(17), (Ni2–O5) = 2.0534(16), (Ni2–N2) = 1.989(2).

bonding donors) and the adjacent O_{Sal} atoms are of significant strength with donor⋯acceptor distances from a very narrow range (from 2.63 to 2.69 Å). This fact has a crucial influence on the deformation of the cubane core; the Ni⋯Ni distances are significantly shorter between the atoms lying within the hydrogen bond bridged faces (3.06–3.10 Å) than those without such intramolecular interaction (3.36 and 3.38 Å). The shorter Ni⋯Ni separations resulted in smaller Ni–O_A–Ni bond angles: 90.7–98.7° *vs.* 102.6–104.0 Å. Such a structural relationship between the intramolecular hydrogen bonding and Ni⋯Ni distances was also found in previously reported Ni_4 cubane compounds.[16]

The intermolecular contacts in **1** are mediated mainly by two hydrogen bonds between the coordinated H_2O molecule and non-coordinated CH_3OH molecule (d(O⋯O) = 2.731(4) Å) and between the non-coordinated CH_3OH molecule and the O_{Sal} atom from the complex molecule (d(O⋯O) = 2.887(4) Å). These two hydrogen bonds form linear supramolecular 1D chains along the crystallographic axis *a* (Fig. S1†).

$(Pr_3NH)_2[Ni_4(L)_4(CH_3COO)_2]$ (2). Single-crystal X-ray diffraction analysis revealed that **2** crystallizes in the monoclinic space group $P2_1/c$. The molecular structure comprises centrosymmetric tetranuclear $[Ni_4(L)_4(CH_3COO)_2]^{2-}$ complex anions (Fig. 3c) and two Pr_3NH^+ cations. It should be noted that the structural motif of the defective dicubane $[Ni_4O_6]$ core was found in several previously reported compounds,[8e,12] but to the best of our knowledge, compound **2** represents the very first example of a defective dicubane $[Ni_4O_6]$ compound with only hexacoordinated Ni^{II} atoms of the $\{NiNO_5\}$ chromophores in the complex molecule (Fig. 3d).

The complex anion in **2** can be also viewed as two parallel and almost planar dinuclear $\{Ni_2(L)_2\}$ subunits symmetrically related to an inversion center. Both subunits are slightly shifted with respect to each other, so the metal atoms are in a rhomb-like arrangement (Fig. 3c). The acetato ligand is bridging the Ni1 and Ni2 atoms (by the oxygen atoms, O_{Ac}) in a *syn–syn* manner (Fig. 3c). The O_{Ac} atoms occupy one of the axial positions in the coordination polyhedra of the Ni1 and Ni2 atoms (d(Ni–O_{Ac}) = 2.1050(16) and 2.0534(16) Å). The remaining axial positions are occupied by the μ-O_A atoms (in the case of Ni1, d(Ni1–O_A) = 2.1810(16) Å) or μ^3-O_A atoms (Ni2, d(Ni2–O_A) = 2.1396(10) Å) from the symmetry related dinuclear subunit. The equatorial planes within the coordination polyhedra of the Ni1 and Ni2 atoms are formed by three donor atoms from the chelating ligand L^{2-} (O_A, O_{Sal} and N_{Im} atoms) and by one bridging O_{Sal} (in the case of Ni1, d(Ni1–O_{Sal}) = 2.0387(15) Å) or O_A (Ni2, d(Ni1–O_A) = 2.0549(16) Å) atom from the adjacent L^{2-} ligand within the dinuclear subunit.

The Ni⋯Ni separations in **2** are in all cases shorter than the sum of van der Waals radii (r_{vdW}(Ni) = 1.63 Å). They are shorter within the $\{Ni_2(L)_2\}$ subunit (d(Ni1⋯Ni2) = 3.0030(4) Å) than between the Ni^{II} atoms which belong to different dimers (d(Ni2⋯$Ni2^i$) = 3.1662(2) Å and d(Ni1⋯$Ni2^i$) = 3.1971(6) Å, symmetry code: (i) $-x$, $1-y$, $1-z$). The Ni–O–Ni angles are (94.12(7) and 96.10(7)°) within the $\{Ni_2(L)_2\}$ subunit smaller than those between the symmetry related Ni atoms in the complex molecule (97.87(7), 97.99(7) and 99.54(7)°).

In the crystal structure of **2**, only one type of significant intermolecular interaction is present: the N–H⋯O hydrogen bond between the Pr_3NH^+ cation and the O_{Sal} atom from the complex anion with the donor⋯acceptor distance 2.820(3) Å.

Theoretical calculations of magnetic parameters

The *ab initio* calculations have become an integral part of the deep-aimed studies of various physical properties of transition metal complexes. Recently, we demonstrated that *ab initio* methods can be successfully used in the predictive role in magnetochemistry, thus helping in postulating trustworthy spin Hamiltonians and guide the theoretical analysis of the experimental magnetic data.[19] Herein, we used the freely available computational package ORCA[20] to predict the dominant terms defining the magnetism of compounds **1** and **2**, that is the magnetic exchange among nickel atoms and also their single-ion contributions to magnetic anisotropy.

DFT calculations of the isotropic exchange. The well-established B3LYP functional together with the polarized triple-ζ quality basis set def2-TZVP(-f) for all atoms was used to evaluate the isotropic exchange constants J by comparing the energy differences between the high spin (HS) and broken-symmetry (BS) spin states. In compound **1**, there are four symmetrically independent nickel atoms with various interatomic distances, so in general, we may expect six different isotropic exchange parameters defined by the following spin Hamiltonian:

$$\begin{aligned}\hat{H} = &-J_{12}(\vec{S}_1\cdot\vec{S}_2) - J_{13}(\vec{S}_1\cdot\vec{S}_3) - J_{14}(\vec{S}_1\cdot\vec{S}_4)\\ &-J_{23}(\vec{S}_2\cdot\vec{S}_3) - J_{24}(\vec{S}_2\cdot\vec{S}_4) - J_{34}(\vec{S}_3\cdot\vec{S}_4)\end{aligned} \quad (1)$$

by the following Ruiz's approach[27] for the calculation of the J-parameters, the expressions for individual J-values were derived as

$$\begin{aligned}J_{12} &= (\Delta_1 + \Delta_2 - \Delta_{12})/6\\ J_{13} &= (\Delta_1 + \Delta_3 - \Delta_{13})/6\\ J_{14} &= (-\Delta_2 - \Delta_3 + \Delta_{12} + \Delta_{13})/6\\ J_{23} &= (\Delta_2 + \Delta_3 - \Delta_{14})/6\\ J_{24} &= (-\Delta_1 - \Delta_3 + \Delta_{12} + \Delta_{14})/6\\ J_{34} &= (-\Delta_1 - \Delta_2 + \Delta_{13} + \Delta_{14})/6\end{aligned} \quad (2)$$

where the energy differences Δ_{ij} are listed in Table S2.† Then, the calculated J_{ij} parameters have the following values: J_{12} = +8.63 cm^{-1}, J_{13} = −6.71 cm^{-1}, J_{14} = +8.62 cm^{-1}, J_{23} = +9.90 cm^{-1}, J_{24} = −6.30 cm^{-1} and J_{34} = +9.67 cm^{-1}. It was already demonstrated by Halcrow *et al.*[8a] and later by Meyer *et al.*[8c] that the isotropic exchange in Ni_4-cubanes correlates with the Ni–O–Ni angle. This is also supported by the herein performed DFT calculations where the linear magneto-structural dependence was found in the form

$$J(cm^{-1}) = 171(1) - 1.72(4)\cdot\alpha(\text{Ni–O–Ni}) \quad (3)$$

as visualized in Fig. 4.

In compound **2**, there are two symmetrically independent nickel atoms and three different superexchange pathways. Therefore, this spin Hamiltonian:

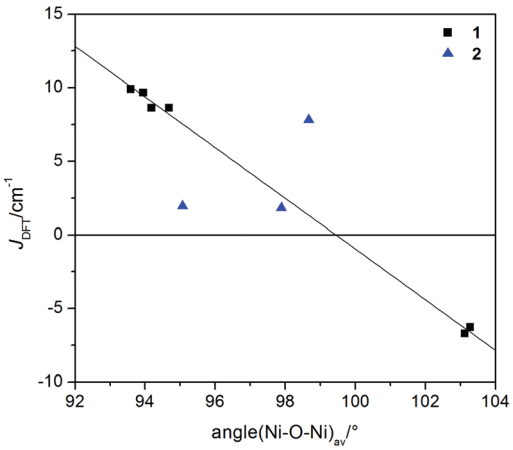

Fig. 4 The DFT derived *J*-parameters for compounds **1** and **2** (full points). The full line corresponds to eqn (3).

$$\hat{H} = -J_1(\vec{S}_1 \cdot \vec{S}_2 + \vec{S}_{1'} \cdot \vec{S}_{2'}) - J_2(\vec{S}_1 \cdot \vec{S}_{2'} + \vec{S}_{1'} \cdot \vec{S}_2) - J_3(\vec{S}_2 \cdot \vec{S}_{2'}) \quad (4)$$

can be used to describe the isotropic exchange within the tetramer of **2**, where J_1 corresponds to the Ni1···Ni2 and Ni1′···Ni2′ pairs with the interatomic distance equal to 3.003 Å, J_2 corresponds to the Ni1···Ni2′ and Ni1···Ni2′ pairs with the interatomic distance equal to 3.197 Å and J_3 corresponds to the Ni2···Ni2′ pair with the interatomic distance equal to 3.166 Å. Again, Ruiz's approach[27] was applied for the calculation of the *J*-parameters as

$$\begin{aligned} J_1 &= (\Delta_1 + \Delta_2 - \Delta_{12})/6 \\ J_2 &= (\Delta_1 - \Delta_2 + \Delta_{12})/6 \\ J_3 &= (\Delta_2 - \Delta_1)/3 \end{aligned} \quad (5)$$

where the energy differences Δ_{ij} are listed in Table S3† and the calculated *J*-parameters adopted the values J_1 = +1.97 cm^{-1}, J_2 = +7.83 cm^{-1} and J_3 = +1.82 cm^{-1}. All the *J*-values suggest ferromagnetic coupling between the nickel atoms in **2**. However, there is no evident correlation between the molecular structure parameters like the Ni–O–Ni angle (Fig. 4) or Ni···Ni distance and the isotropic exchange parameters (Fig. S2, ESI†).

Multi-reference calculations of the single-ion zero-field splitting tensors. The progress in theoretical methods enabled us to analyze also single-ion zero-field splitting in compounds **1** and **2** by multireference state average complete active space self-consistent field (SA-CASSCF) wavefunctions complemented by the N-electron valence state perturbation theory (NEVPT) with CAS(8,5) active space. We used this method successfully to analyze the magnetic anisotropy in other 3d metal complexes.[21] However, the analysis of ZFS in polynuclear species is not an easy task and usually is done either by substituting some paramagnetic metal atoms by diamagnetic ones, or by extracting molecular fragments with only one metal atom. Herein, we tested these approaches for compound **2** and calculated the *D*- and g-tensors on the Ni1 atom using the molecular fragments (a) $[NiZn_3(L)_4(CH_3COO)_2]^{2-}$, (b) $[Ni(L)_3(CH_3COO)]^{5-}$, (c) $[Ni(L)(PhO)_2(CH_3COO)]^{3-}$ and (d) $[Ni(L)(CH_3O)_2(CH_3COO)]^{3-}$ (see Fig. S3 for details, ESI†).

We used the fact that only one L^{2-} ligand binds in a tridentate fashion to the Ni1 atom, so in the molecular fragments (c) and (d) the monodentate ligands L were replaced either by PhO^- or CH_3O^- moieties (Fig. S3, ESI†). Reducing the number of atoms involved in the molecular fragments of **2** resulted in speeding up the CASSCF/NEVPT2 calculations in the following order (a) < (b) < (c) < (d). The effect of reducing the size of the molecular fragment on the calculations of the *D*-tensor parameters *D* and *E* is documented as: D = +9.62 cm^{-1}, E/D = 0.18 for (a), D = +9.43 cm^{-1}, E/D = 0.21 for (b), D = +9.58 cm^{-1}, E/D = 0.21 for (c) and D = +8.02 cm^{-1}, E/D = 0.19 for (d). Thus, the calculations proved that the approaches (a–c) resulted in almost the same ZFS parameters, only in the case of (d) the *D*-parameter is slightly lower, which can be explained by the difference in the electronic properties of phenyl/methyl groups (–I/+I inductive effect), hence different electron densities on the oxygen donor atom. Therefore, the justified approach (c) based on using mononuclear fragments where monodentate ligands L^{2-} are replaced by phenolato ligands was used to calculate the ZFS parameters for all the nickel atoms in compounds **1** and **2** and the results are summarized in Table 1.

The absolute value of the axial single-ion parameter $|D|$ varies between 8.5 and 13.5 cm^{-1} and also considerable rhombicity (E/D) was found for all the nickel atoms in the studied compounds **1** and **2** (Table 1). The calculated *g*-parameters are in a narrow interval, g = 2.18–2.30. The individual *g*-tensor and *D*-tensor axes are visualized in Fig. S4.† In all the molecular fragments, the *g*-tensor axes coincide with the *D*-tensor axes, and under conditions that the ZFS-tensor defines the coordination axes *X*, *Y* and *Z*, the following relationships hold true for the *g*-components: $g_x = g_2$, $g_y = g_3$, $g_z = g_1$ for $D > 0$, and $g_x = g_2$, $g_y = g_1$, $g_z = g_3$ for $D < 0$. This is in agreement with the simplified relationships (eqn (6)) derived from ligand field theory using second-order perturbation theory and so called Λ-tensor[22]

$$\begin{aligned} D &= -\lambda(g_x + g_y - 2g_z)/4 \\ E &= -\lambda(g_y - g_x)/4 \end{aligned} \quad (6)$$

where λ is the spin-orbit splitting parameter, $\lambda(Ni^{2+})$ = −315 cm^{-1}.

Next, we need to discuss thoroughly the *D*-tensor orientations in each studied compound, because within the spin

Table 1 The CASSCF/NEVPT2/def2-TZVP(-f) calculated ZFS parameters for the nickel atoms in compounds **1–2**

	Atom	D (cm^{-1})	E/D	g_1	g_2	g_3
1	Ni1	+12.4	0.194	2.185	2.265	2.297
	Ni2	+12.3	0.315	2.177	2.245	2.298
	Ni3	+13.5	0.189	2.176	2.263	2.298
	Ni4	+12.5	0.197	2.181	2.260	2.294
2	Ni1	+9.58	0.209	2.206	2.264	2.292
	Ni2	−8.45	0.309	2.199	2.236	2.279

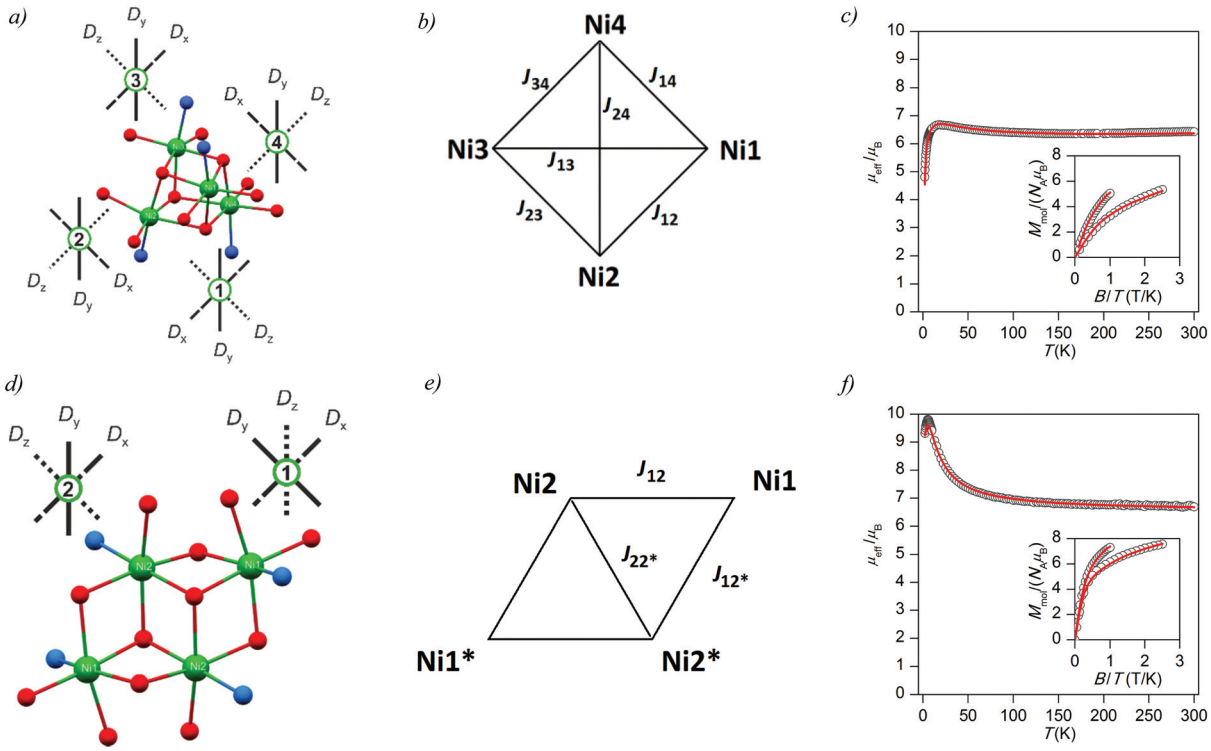

Fig. 5 Magnetic data for compounds **1** (c) and **2** (f) showing the temperature dependence of the effective magnetic moment calculated from molar magnetization measured at B = 0.1 T and reduced isothermal magnetizations measured at T = 2 and 5 K in the insets; full lines correspond to the calculated data with parameters in text. Representations of the structural cores and *ab initio* calculated single-ion zero-field splitting tensor axes for **1** (a) and **2** (d). Schemes of the magnetic exchange pathways in cubane-like compound **1** (b) and defective dicubane-like compound **2** (e).

Hamiltonian formalism, the co-linearity of the local D-tensors is generally assumed. The inspection of the local D-tensor axes labelled as DX, DY and DZ in **1** (Fig. S4†) showed that for all four nickel atoms (Ni1···Ni4), the DX axis coincides with O_L–Ni–O_L, the DY axis coincides with N_{Im}–Ni–O_{Ph} and the DZ axis coincides with O_{Ph}–Ni–O_{Solv}, where O_L is the oxygen donor atom from the L^{2-} ligand bound in the terminal tridentate fashion to the nickel atom, O_{Ph} is the oxygen donor atom from the L^{2-} ligand bound in the bridging monodentate fashion to the nickel atom and O_{Solv} is the oxygen donor atom from the CH_3OH/H_2O ligand. If we assume idealized S_4 symmetry of the Ni_4 molecular fragment of **1**, then we can schematically visualize in Fig. 5a the orientation of the local axes of all the nickel atoms. Under this assumption holds $\mathbf{D}_1 \equiv \mathbf{D}_3$ and $\mathbf{D}_2 \equiv \mathbf{D}_4$. If the molecular axes are made identical to $\mathbf{D}_1$ (or $\mathbf{D}_3$), then the local axes of $\mathbf{D}_2$ are transformed into the molecular coordinate system ($\mathbf{D'}_2$) using $C_4(y)$ operation of the symmetry as

$$\mathbf{D}_2 \xrightarrow{C_4(y)} \mathbf{D'}_2$$
$$\begin{pmatrix} D_{xx} & 0 & 0 \\ 0 & D_{yy} & 0 \\ 0 & 0 & D_{zz} \end{pmatrix} \xrightarrow{C_4(y)} \begin{pmatrix} D_{zz} & 0 & 0 \\ 0 & D_{yy} & 0 \\ 0 & 0 & D_{xx} \end{pmatrix} \quad (7)$$

and analogously for $\mathbf{D}_4$. Then, the axial (D) and rhombic (E) ZFS parameters, which are defined as

$$D = (3/2)D_{zz}$$
$$E = (D_{xx} - D_{yy})/2 \quad (8)$$

are transformed for the Ni2 and Ni4 atoms into the molecular coordination system as

$$D' = (-D + 3E)/2$$
$$E' = (D + E)/2 \quad (9)$$

where these general relationships

$$D_{xx} = -D/3 + E$$
$$D_{yy} = -D/3 - E$$
$$D_{zz} = 2D/3 \quad (10)$$

were utilized. The tetranuclear molecular fragment of **2** possesses the C_i point group symmetry and the examination of the local D-tensor axes revealed that for the Ni1 atom (similarly to Ni1^i), the DX axis coincides with O_L–Ni–O_L, the DY axis coincides with N_{Im}–Ni–O_{Ph} and the DZ axis coincides with O_{Ph}–Ni–O_{ac}, where O_{ac} is the oxygen donor atom from the acetato ligand. In the case of the Ni2 atom (similarly to Ni2^i), DY and DZ axes are interchanged (Fig. S4, ESI†). The orientation of these local axes of all nickel atoms is schematically visualized in Fig. 5d. Again, if the molecular axes are made identical to $\mathbf{D}_1$, then the local axes of $\mathbf{D}_2$ are transformed into

the molecular coordinate system ($\mathbf{D'}_2$) using $C_4(x)$ operation of the symmetry as

$$\mathbf{D}_2 \xrightarrow{C_4(x)} \mathbf{D'}_2$$
$$\begin{pmatrix} D_{xx} & 0 & 0 \\ 0 & D_{yy} & 0 \\ 0 & 0 & D_{zz} \end{pmatrix} \xrightarrow{C_4(x)} \begin{pmatrix} D_{xx} & 0 & 0 \\ 0 & D_{zz} & 0 \\ 0 & 0 & D_{yy} \end{pmatrix}. \quad (11)$$

Now, the local D and E ZFS parameters for the Ni2 atom are transformed into the molecular coordination system as

$$D' = (-D - 3E)/2$$
$$E' = (-D + E)/2. \quad (12)$$

As the operation of inversion has no effect on the D-tensor, the local D-tensors of $Ni1^i$ and $Ni2^i$ atoms have the same properties as for Ni1 and Ni2 atoms.

Description of magnetic properties. The temperature and field dependent magnetic properties of **1** and **2** are depicted in Fig. 5. Variable temperature measurements of μ_{eff}/μ_B *vs.* T for compounds **1** and **2** show a similar trend. The room temperature experimental values, $6.7\mu_B$ for **1** and **2**, are higher than the theoretical value of the effective magnetic moment for four non-interacting Ni^{II} atoms with $S_i = 1$ is equal to $5.7\mu_B$ for $g = 2.0$ due to the contribution of the angular momentum to the ground spin state ($g > 2.0$). On lowering the temperature, μ_{eff}/μ_B gradually increases reaching the value of 6.7 (compound **1**) and 9.8 (compound **2**). Further cooling leads to a decrease of the μ_{eff}/μ_B value to 4.8 (compound **1**) and 9.3 (compound **2**) at 1.9 K. The high temperature behavior for compounds **1** and **2** is typical of compounds with prevailing intracluster ferromagnetic coupling and low temperature data suggest the presence of magnetic anisotropy of the Ni^{II} atoms. The lower effective magnetic moment at low temperature in **1** than in **2** can be explained by the presence of intracluster antiferromagnetic coupling as derived from DFT calculations. Moreover, from the field-dependent magnetization data shown in Fig. 5 we can deduce that the ferromagnetic coupling is dominant in compound **2**, where $M_{mol}/N_A\mu_B$ almost reaches the value of 8.0 while the high-field limit is lower in compound **1** due to the presence of intracluster antiferromagnetic coupling and zero-field splitting.

The analysis of the magnetic data for compound **1** is based on the following spin Hamiltonian (Fig. 5b)

$$\hat{H} = -\sum_{i=1}^{4}\sum_{j=i+1}^{4} J_{ij}(\vec{S}_i \cdot \vec{S}_i) + \sum_{i=1}^{4} \vec{S}_i \cdot \overline{\overline{D}}_i \cdot \vec{S}_i + \mu_B B_a \sum_{i=1}^{4} g\hat{S}_a \quad (13)$$

where the isotropic, ZFS and Zeeman terms were included. In order to reduce the number of free parameters, and inspired by the results of the above-mentioned *ab initio* calculations, we parametrized the J_{ij}-value analogously to eqn (3) using

$$J(\mathrm{cm}^{-1}) = a - b \cdot \alpha(\mathrm{Ni\text{–}O\text{–}Ni}) \quad (14)$$

Furthermore, the CASSCF/NEVPT2 calculations showed that the local ZFS parameters are very similar for all four symmetrically independent nickel atoms (Table 1), so the following restriction was applied: $D_1 = D_2 = D_3 = D_4 = D_{loc}$ and $E_1 = E_2 = E_3 = E_4 = E_{loc}$. Also, the local ZFS parameters of $\mathbf{D}_2$ and $\mathbf{D}_4$ were transformed according to eqn (9) in the spin Hamiltonian (eqn (13)). Moreover, only the isotropic g-value was assumed, because the *ab initio* calculated g-parameters do not possess large anisotropy. Thus, we are left with only five independent parameters for the fitting procedure, in which simultaneously both temperature and field dependent data were analyzed. As a result, the best-fitted parameters were obtained: $a = 171.0$, $b = -1.721$, $g = 2.147$, $D_{loc} = +14.5\ \mathrm{cm}^{-1}$, $E_{loc}/D_{loc} = 0.267$ and $\chi_{TIP} = 12.9 \times 10^{-9}\ \mathrm{m}^3\ \mathrm{mol}^{-1}$ (Fig. 5c), where χ_{TIP} stands for temperature-independent paramagnetism (*note*: the estimation of the standard deviations resulted in: $a = 171(9)$, $b = -1.72(9)$, $g = 2.147(4)$, $D_{loc} = +14.5(3)\ \mathrm{cm}^{-1}$, $E_{loc} = 3.9(2)\ \mathrm{cm}^{-1}$).[23] Then, the individual J-values were calculated as $J_{12} = +8.05\ \mathrm{cm}^{-1}$, $J_{13} = -6.48\ \mathrm{cm}^{-1}$, $J_{14} = +8.91\ \mathrm{cm}^{-1}$, $J_{23} = +9.93\ \mathrm{cm}^{-1}$, $J_{24} = -6.74\ \mathrm{cm}^{-1}$ and $J_{34} = +9.32\ \mathrm{cm}^{-1}$. All the fitted parameters are in very good concordance with the theoretical ones showing the power of *ab initio* theoretical calculations in the analyses of such complicated systems.

The analysis of the magnetic data for compound **2** is based on the slightly modified spin Hamiltonian (Fig. 5e)

$$\hat{H} = -J_1(\vec{S}_1 \cdot \vec{S}_2 + \vec{S}_{1'} \cdot \vec{S}_{2'}) - J_2(\vec{S}_1 \cdot \vec{S}_{2'} + \vec{S}_{1'} \cdot \vec{S}_2) - J_3(\vec{S}_2 \cdot \vec{S}_{2'}) + \sum_{i=1}^{4} \vec{S}_i \cdot \overline{\overline{D}}_i \cdot \vec{S}_i + \mu_B B_a \sum_{i=1}^{4} g\hat{S}_a. \quad (15)$$

The situation in this complex is more complicated by the fact that there is no magneto-structural correlation for the J-parameters. From the DFT calculations of the J-values, we can conclude that J_1 and J_3 are almost equal, so we can apply the restriction that $J_1 = J_3$, and that J_2 is four-times larger than J_1 or J_3, so we also applied the restriction that $J_2 = 4J_1$. In order to further reduce the number of free parameters, the CASSCF/NEVPT2 calculations were also utilized in such a way that based on the opposite values of the local D_1 and D_2 parameters, these simplifications were used: $D_1 = D_{1'} = D_{loc}$, $D_2 = D_{2'} = -D_{loc}$ and analogously $E_1 = E_{1'} = E_{loc}$, $E_2 = E_{2'} = -E_{loc}$. Then, the transformation of $\mathbf{D}_2$ and $\mathbf{D}_{2'}$ tensors was applied using eqn (12) similarly as in the case of **1**. The fitting procedure resulted in $J_1 = J_3 = +2.61\ \mathrm{cm}^{-1}$, $J_2 = +10.5\ \mathrm{cm}^{-1}$, $D_{loc} = +8.60\ \mathrm{cm}^{-1}$, $E_{loc}/D_{loc} = 0.277$ and $g = 2.309$ (Fig. 5f) (*note*: the estimation of the standard deviations resulted in: $J_1 = J_3 = +2.61(4)\ \mathrm{cm}^{-1}$, $D_{loc} = +9(3)\ \mathrm{cm}^{-1}$, $E_{loc} = 2(3)\ \mathrm{cm}^{-1}$ and $g = 2.309(3)$).[22] These derived parameters are in good conformity with the theoretically predicted values, however, the estimated standard deviations of ZFS parameters D_{loc} and E_{loc} are rather large showing smaller sensitivity of the experimental magnetic data to the variation of these parameters. Nevertheless, such uncertainty of the fitted ZFS parameters underlines the importance of *ab initio* methods in the theoretical analysis of the magnetic properties of polynuclear species.

It is evident from the magnetic analysis that the structural variations found in compounds **1** and **2** led to enhanced differences in their magnetic behavior despite a very similar chemical

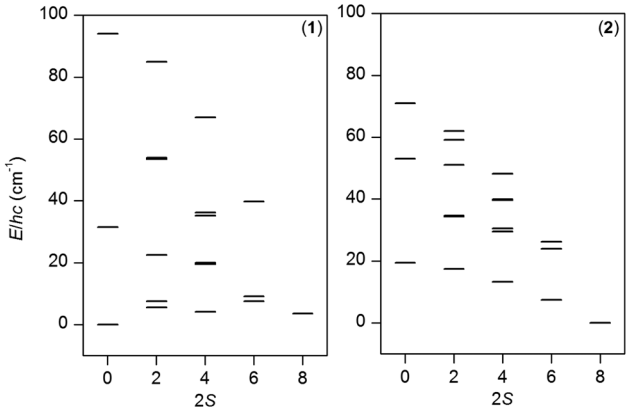

Fig. 6 The energy patterns for compounds **1** and **2** calculated within the isotropic exchange limit with the J_{ij}-parameters listed in the text and setting all D and E parameters to zero.

composition. In order to better understand the interplay between the ferromagnetic and antiferromagnetic exchange interactions within these compounds, the energy levels were plotted as a function of the final spin S under the condition that the spin Hamiltonian is isotropic (all ZFS parameters are zero) – Fig. 6.

From this plot it is obvious that the ground state for compound **1** is $S = 0$ and there are close-lying states (<5 cm^{-1}) with $S = 4$ and $S = 2$. In contrast, ferromagnetic interactions in compound **2** led to the ground state with the maximum spin, $S = 4$, and the first excited state with $S = 3$ is separated by energy difference $\Delta E = 7.4$ cm^{-1} (10.7 K). Furthermore, we have depicted a three-dimensional plot of the molar magnetization for **2** (Fig. 7a) from which is evident that there is an axial type of the magnetic anisotropy with a small rhombicity. Therefore, it seems appropriate to utilize giant spin approximation and fit the isothermal magnetization data for **2** with the spin Hamiltonian for the ground spin state $S = 4$ in order to alternatively determine the magnetic anisotropy of the ground spin state with eqn (16)

$$\hat{H} = D\left(\hat{S}_z^{\,2} - \hat{S}^2/3\right) + \mu_B B_a g \hat{S}_a. \qquad (16)$$

The results of the analysis are shown in Fig. 7b and the obtained parameters are $D = -0.81$ cm^{-1} and $g = 2.17$ (*note*: the estimation of the standard deviation resulted in: $D = -0.81(3)$ cm^{-1} and $g = 2.17(1)$).[22] These values are comparable to the previously reported Ni_4 SMMs as outlined in Table 2. However, such large D-values result in ZFS of the $S = 4$ spin state into $|4,0\rangle$, $|4,\pm1\rangle$, $|4,\pm2\rangle$, $|4,\pm3\rangle$ and $|4,\pm4\rangle$ states with the energy separations equal to 0, D, 4D, 9D, and 16D, respectively. Thus, the ground state $|4,\pm4\rangle$ is separated from the highest excited state $|4,0\rangle$ by energy equal to $16D = 13.0$ cm^{-1} and this value is larger than calculated separation 7.4 cm^{-1} between $S = 4$ and $S = 3$ states in the isotropic limit (Fig. 6). Indeed, the detailed inspection of the low-lying energy levels resulting from full multi-spin Hamiltonian in eqn (15) and from giant spin

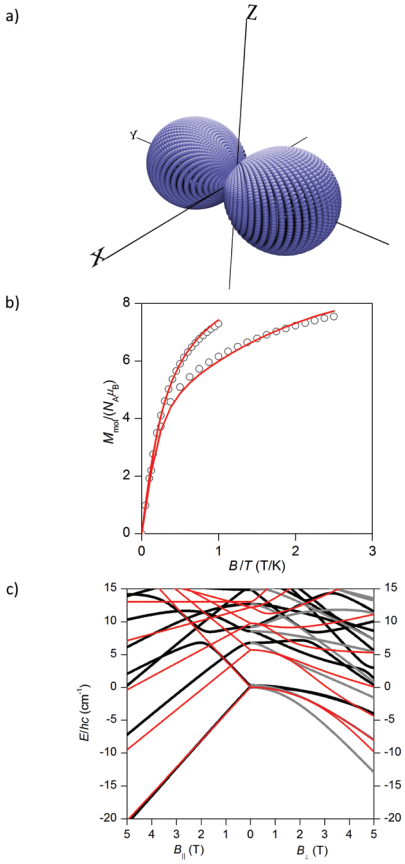

Fig. 7 (a) The 3D plot of the molar magnetization calculated for **2** with multi-spin Hamiltonian in eqn (15) for $B = 0.5$ T at $T = 2$ K. (b) The reduced isothermal magnetization data for **2** measured at $T = 2$ and 5 K fitted with the single-ion zero-field splitting spin Hamiltonian for $S = 4$ (eqn (16)). Empty circles – experimental data, full lines – calculated data with $D = -0.81$ cm^{-1} and $g = 2.17$. (c) The comparison of the lowest energy levels of **2** calculated with multi-spin Hamiltonian in eqn (15) (black and grey lines) and with giant spin approximation Hamiltonian in eqn (16) (red lines). The $B_{\|}$ indicates the direction of the magnetic field parallel to the easy axis, whereas $B_{\perp}$ indicates the direction of the magnetic field perpendicular to the easy axis of the system.

approximation Hamiltonian in eqn (16) shows that only the lowest energy levels are well recovered by the latter model (Fig. 7c). Moreover, it is evident that there is a strong mixing of different spin levels due to ZFS terms, so called S-mixing,[24] and therefore the giant spin approximation would require inclusion of the higher order Steven's operators for ZFS to achieve even better description of low-lying states, which was also discussed for another Ni_4 compound, $[Ni_4(hmp)_4(dmb)_4Cl_4]$.[25] To conclude, both the analyses showed that there is the axial type of the magnetic anisotropy in **2**, however the utilization of the giant spin approximation is on the edge due to large mixing of the ground state $S = 4$ with the excited state $S = 3$ induced by ZFS.

The above discussed analysis of the static magnetic properties of **1–2**, encouraged us to measure also AC susceptibility data for compound **2**, but there was no out-of-phase signal in zero static magnetic field. However, the field dependent

Table 2 List of the published Ni^{II}_4 SMMs with their basic SMM characteristics[a]

Compound	D (cm^{-1})	U_{eff} (cm^{-1})	τ_0 (s)	Ref.
$[Ni_4(hmp)_4(CH_3OH)_4Cl_4]$[b]	−0.60			5*a*
$[Ni_4(hmp)_4(CH_3CH_2OH)_4Cl_4]$	−0.60	5.00	9.5×10^{-8}	5*a* and 6*g*
$[Ni_4(hmp)_4(dmb)_4Cl_4]$	−0.61	1.39	6.3×10^{-3}	5*a*,*d*
$[Ni_4(hmp)_4(dmp)_4Cl_4]$[b]	−0.61			5*f*
$[Ni_4(hmp)_4(chp)_4Cl_4]$[b]	−0.59			5*d*
$[Ni_4(hmp)_4(dmb)_4Br_4]$[b]	−0.56			5*d*
$[Ni_4(^tBuhmp)_4(dmb)_4Cl_4]$[b]	−0.68			5*d*
$[Ni_4(H_2thme)_4(CH_3CN)_4](NO_3)_4{\cdot}1.33NaNO_3$ [b]	−0.43			5*b*
$[Ni_4(Hidm)_4Cl_4]$[b]	−0.75			5*e*
$[Ni_4(Hpthtp)_4Cl_8]$	−0.44	20.1	1.64×10^{-9}	6*k*
$[Ni_4(Hmpp)_4Cl_8]$[b]	−0.88			6*j*
$[Ni_4(Hmpp)_4OH_4Cl_4]$[b]	−0.63			6*j*
$[Ni_4(mpzph)_4(OH)(CH_3O)_3(CH_3OH)_3](CH_3OH)$[b]	−0.26		1.50×10^{-6}	17*a*
$(Pr_3NH)_2[Ni_4(L)_4(CH_3COO)_2]$ (**2**)	−0.81	2.3–4.7	$79.7–0.261 \times 10^{-6}$	This work

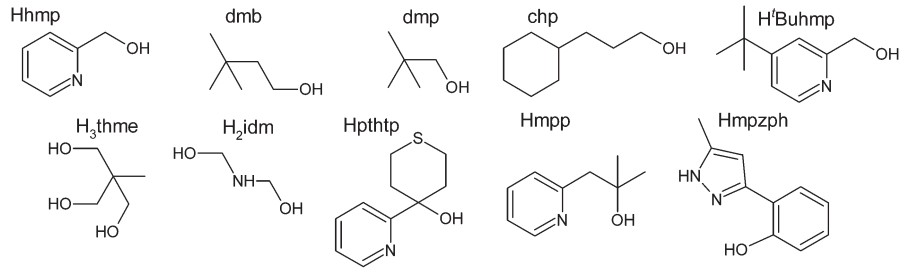

[a] SMM behavior confirmed by magnetic hysteresis measurement, AC susceptibility data not available. [b] Hhmp = (pyridin-2-yl)methanol; dmb = 3,3-dimethylbutan-1-ol; dmp = 2,2-dimethylpropan-1-ol; dmp = 3-cyclohexylpropan-1-ol; H^{t}Buhmp = (4-*tert*-butylpyridine-2-yl)methanol; H_3thme = 2-(hydroxymethyl)-2-methylpropane-1,3-diol; H_2idm = iminodimethanol; Hpthtp = 4-(pyridin-2-yl)tetrahydro-2*H*-thiopyran-4-ol; Hmpp = 2-methyl-1-(pyridin-2-yl)propan-2-ol; Hmpzph = 2-(5-methyl-1*H*-pyrazol-3-yl)phenol.

measurement performed at T = 1.9 K confirmed a slow-relaxation of magnetization only in **2** (Fig. S5, ESI†) and for that reason, AC susceptibility was acquired in the non-zero static field, B_{dc} = 0.5 T at low temperatures as shown in Fig. 8. Note: AC susceptibility data were also taken for compound **1** in zero and non-zero static fields, but no out-of-phase signal was detected, which indirectly confirmed our outcomes from magnetic analysis.

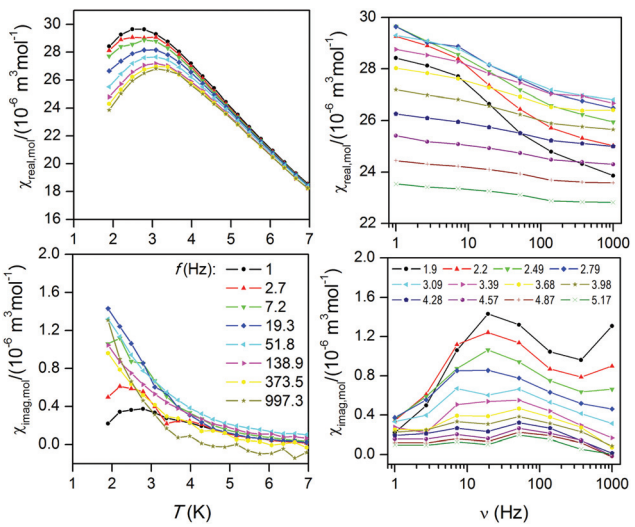

Fig. 8 In-phase χ_{real} and out-of-phase χ_{imag} molar susceptibilities for **2** at the applied external field B_{dc} = 0.5 T shown as a function of temperature (left) and ac frequency ν (right). Lines serve as guide to the eye.

Unfortunately, we did not observe clear maxima on out-of-phase susceptibilities for **2** down to 1.9 K, so the standard procedure for constructing the Argand (Cole–Cole) diagram was not applicable. However, at least the approximate relationship[26]

$$\ln(\chi''/\chi') = \ln(2\pi f\tau_0) + U/kT \quad (17)$$

for the extraction of the relaxation time and spin reversal barrier (U) was applied to very low temperature data and higher applied frequencies as visualized in Fig. S6.† As a result, we obtained sets of the following parameters: $\tau_0 = 7.97 \times 10^{-5}$ s, U = 3.3 K for f = 19.3 Hz, $\tau_0 = 2.44 \times 10^{-5}$ s, U = 3.6 K for f = 51.8 Hz, $\tau_0 = 7.83 \times 10^{-6}$ s, U = 3.5 K for f = 138.9 Hz, $\tau_0 = 1.85 \times 10^{-6}$ s, U = 4.2 K for f = 373.5 Hz $\tau_0 = 2.61 \times 10^{-7}$ s, and U = 6.7 K for f = 997.3 Hz. The variation of the fitted parameters can be explained by the distribution of relaxation processes, which is usually treated by the parameter α in one-component Debye's model[1] and which is absent in this simplified model. The spin reversal barrier U spans the interval of 3.3–6.7 K (2.3–4.7 cm^{-1}), which is close to those reported for the cubane-like Ni_4 SMMs listed in Table 2, except for the compound $[Ni_4(Hpthtp)_4Cl_8]$ in the literature,[6k] where reported U = 20.1 cm^{-1} is much larger than the theoretically predicted value, $U = |D|{\cdot}S^2 = |-0.44|{\cdot}4^2 = 7.04$ cm^{-1}. In the case of compound **2**, the determined barrier is lower than theoretically

predicted, $U = |D| \cdot S^2 = |-0.81| \cdot 4^2 = 13.0\ cm^{-1}$, which may be explained by simplicity of the giant spin approximation model in deriving the *D*-parameter as discussed above and also due to more complex relaxation phenomena taking place (combination of Orbach, Raman and direct processes), as was already observed in the other previously reported Ni_4 SMMs (Table 2).

Conclusions

To conclude, the utilization of the tridentate Schiff base ligand H_2L (2-hydroxy-phenylsalicylaldimine) and $Ni(CH_3COO)_2 \cdot 4H_2O$, in different reaction solvent ratios, led to the synthesis of two structurally different tetranuclear complexes **1** and **2**. Single-crystal X-ray structural analysis revealed that compound **1** contains a cubane-like $[Ni_4O_4]$ core (a mixture of $CH_3OH : CH_2Cl_2$ in vol. ratio 1 : 3 was used), while compound **2** involves a defective dicubane-like $[Ni_4O_6]$ core (CH_2Cl_2 only). Consequently, the solvent molecules were incorporated in the structure of compound **1** and they are involved in mediation of intra and intermolecular hydrogen bonds. Compound **2** represents the very first example of tetranuclear Ni^{II} complex with a defective dicubane core and with all the Ni^{II} atoms being hexacoordinate.

The variable temperature magnetic data suggested the presence of prevailing intracluster ferromagnetic coupling (**1** and **2**). However, more thorough analysis revealed the competition between the antiferromagnetic and ferromagnetic intracluster interactions in compound **1** which resulted in the $S = 0$ ground spin state. This is in stark contrast to **2** with its $S = 4$ ground spin state due to solely ferromagnetic coupling. Furthermore, the energy states in both compounds are affected by significant magnetic anisotropy of the metal atoms, which reflects the structural variations in **1** and **2**. The *ab initio* CASSCF/NEVPT2 calculations of the isotropic exchange parameters (J_{ij}) using the DFT and single-ion zero-field splitting parameters (D_i, E_i) played the key role in the advanced magnetic analysis of these compounds, which resulted in the trustworthy parameter set. This was also achieved by simultaneous fitting of temperature and field dependent magnetic data.

This work clearly shows the difficulty in the rational design of highly anisotropic polynuclear complexes as candidates for SMMs. Nevertheless, the field induced SMM behavior found in compound **2** opens a new perspective for the preparation of tetranuclear compounds with a defective dicubane-like topology and ferromagnetic exchange interactions acting as nanomagnets.

Experimental section

Synthesis

All used chemicals and solvents were purchased from commercial sources and used without any further purification.

$[Ni_4(L)_4(CH_3OH)_3(H_2O)] \cdot CH_3OH$ (1). A green solution of $Ni(CH_3COO)_2 \cdot 4H_2O$ (0.06 g, 0.23 mmol) in CH_3OH (10 cm^3) was added to an orange solution of the H_2L ligand (0.05 g, 0.23 mmol) in CH_2Cl_2 (30 cm^3). The dark red reaction mixture was stirred for 15 minutes after which a solution of tripropylamine (0.07 g, 0.48 mmol) in CH_3OH (2 cm^3) was slowly added. The resultant mixture was stirred and refluxed for additional 15 minutes and then it was filtered. The mother liquor was then allowed to evaporate slowly at room temperature. After a few days, brownish green prism shaped crystals were collected by filtration, washed with diethyl ether and dried in a vacuum desiccator. Yield: 50% (36 mg). Elemental analysis (crystalline phase): Anal. Calcd for $C_{56}H_{54}N_4O_{13}Ni_4$ (1225.84): C, 54.9; H, 4.4; N, 4.6. Found: C, 55.2; H, 4.0; N, 4.7. FT-IR, (ATR, cm^{-1}): 3606(w), 3500(w), 3338(w), 3055(m), 3007(m), 2927(m), 1613(s), 1598(s), 1586(s), 1533(m), 1477(m), 1462(s), 1437(m), 1382(m), 1340(m), 1289(m), 1238(s), 1218(m), 1170(m), 1148(s), 1124(m), 1107(m), 1035(m), 918(m), 824(m), 739(s), 649(w), 617(m), 567(w), 518(m).

$(Pr_3NH)_2[Ni_4(L)_4(CH_3COO)_2]$ (2). An orange solution of H_2L (0.10 g, 0.47 mmol) in 10 cm^3 CH_2Cl_2 was added to a green suspension of $Ni(CH_3COO)_2 \cdot 4H_2O$ (0.18 g, 0.70 mmol) in 30 cm^3 CH_2Cl_2. The resulting green suspension was stirred and refluxed. The addition of tripropylamine (0.14 g, 0.94 mmol) in a small amount of CH_2Cl_2 (2 cm^3) after 15 minutes resulted in a change of color to dark red. The mixture was refluxed for 15 minutes and then filtered. The mother liquor was left undisturbed to evaporate slowly at room temperature. After a few days, green prism shaped crystals were filtered and dried in a vacuum desiccator. Yield: 44% (40 mg). Elemental analysis (crystalline phase): Anal. Calcd for $C_{74}H_{86}N_6O_{12}Ni_4$ (1486.31): C, 59.8; H, 5.8; N, 5.7. Found: C, 59.6; H, 5.8; N, 5.5. FT-IR (ATR; cm^{-1}): 3048(m), 2972(m), 2876(m), 2666(w), 1612(m), 1596(m), 1568(s), 1532(m), 1466(s), 1441(m), 1403(m), 1381(m), 1346(m), 1297(s), 1282(s), 1254(m), 1322(m), 1166(m), 1147(s), 1121(m), 1104(w), 1032(m), 957(w), 916(m), 826(m), 740(s), 655(w), 614(w), 511(m).

Equipment, measurements and software

Elemental analysis was performed on a Thermo Scientific FLASH 2000 CHNS-O Analyser. Infrared spectra of the compounds were recorded with a ThermoNicolet Nexus 670 FT-IR spectrometer using the ATR technique on the diamond plate in the region 4000–400 cm^{-1}. Temperature dependent (T = 1.9–300 K, B = 0.1 T) and field dependent (B = 0–7 T, T = 2 and 5 K) magnetic measurements were carried out on an SQUID magnetometer (MPMS, Quantum Design) on polycrystalline samples. The data were corrected for the diamagnetism of the constituents.

X-ray diffraction analysis

Single crystal X-ray diffraction data are listed in Table S1.† The data were recorded on an Oxford diffraction Xcalibur 2 CCD diffractometer with a Sapphire CCD detector, sealed tube (Mo Kα radiation, Kα = 0.71073 Å) and equipped with an Oxford Cryosystems nitrogen gas-flow apparatus. The CrysAlis program package (version 1.171.33.52, Oxford Diffraction) was

used for data collection and reduction.[27] The molecular structures were solved by direct methods SHELX-2014 and all non-hydrogen atoms were refined anisotropically on F^2 using the full-matrix least-squares procedure SHELXL-97.[28] All the hydrogen atoms were found in differential Fourier maps and their parameters were refined using a riding model with $U_{iso}(H)$ = 1.2 (CH, CH_2, OH) or 1.5U_{eq} (CH_3).

Theoretical methods

Ab initio theoretical calculations were performed with the ORCA 3.0.3 computational package.[29] Single point DFT energy calculations based on X-ray geometries were done using the B3LYP functional.[30] The isotropic exchange constants J were calculated by comparing the energies of high-spin (HS) and broken-symmetry (BS) spin states using Ruiz's approach.[31] Calculations of the ZFS parameters were performed using the state average complete active space self-consistent field (SA-CASSCF)[32] wave functions complemented by the N-electron valence second order perturbation theory (NEVPT2).[33] The active spaces of the CASSCF calculations comprises five metal-based d-orbitals and eight electrons, CAS(8,5). In the state averaged approach all multiplets for the given electron configuration were equally weighted, which means 10 triplet and 15 singlet states. The ZFS parameters, based on dominant spin–orbit coupling contributions from excited states, were calculated through the quasi-degenerate perturbation theory (QDPT),[34] in which approximations to the Breit–Pauli form of the spin-orbit coupling operator (SOMF approximation)[35] and the effective Hamiltonian theory[36] were utilized. In all calculations, the polarized triple-ζ quality basis set (def2-TZVP(-f)) proposed by Ahlrichs and co-workers was used for all atoms.[37] We also used the RI approximation with the decontracted auxiliary def2-TZV/J or def2-TZV/C Coulomb fitting basis sets and the chain-of-spheres approximation to exact exchange.[38] Increased integration grids (Grid5 in ORCA convention) and tight SCF convergence criteria were used in all calculations.

Acknowledgements

We acknowledge the financial support from the National Programme of Sustainability I (LO1305) of the Ministry of Education, Youth and Sports of the Czech Republic, and from Palacký University in Olomouc (PrF_2015_019 and PrF_2016_007). I.N would like to acknowledge the Grant Agency of the Czech Republic (GAČR 13-27355P) for financial support.

Notes and references

1 (*a*) R. Sessoli, D. Gatteschi, A. Caneschi and M. A. Novak, *Nat.*, 1993, **365**, 141; (*b*) L. Thomas, F. Lionti, R. Ballou, D. Gatteschi, R. Sessoli and B. Barbara, *Nat.*, 1996, **383**, 145; (*c*) M. N. Leuenberger and D. Loss, *Nat.*, 2001, **410**, 789; (*d*) S. Wang, J. L. Zuo, H. C. Zhou, H. J. Choi, Y. X. Ke, J. R. Long and X. Z. You, *Angew. Chem., Int. Ed.*, 2004, **43**, 5940; (*e*) M. H. Zeng, M. X. Yao, H. Liang, W. X. Zhang and X. M. Chen, *Angew. Chem., Int. Ed.*, 2007, **46**, 1832; (*f*) C. J. Milios, A. Vinslava, P. A. Wood, S. Parsons, W. Wernsdorfer, G. Christou, S. P. Perlepes and E. K. Brechin, *J. Am. Chem. Soc.*, 2007, **129**, 8; (*g*) S. Bertaina, S. Gambarelli, T. Mitra, B. Tsukerblat, A. Müller and B. Barbara, *Nat.*, 2008, **453**, 203; (*h*) M. Mannini, F. Pineider, P. Sainctavit, C. Danieli, E. Otero, C. Sciancalepore, A. M. Talariano, M.-A. Arrio, A. Cornia, D. Gatteschi and R. Sessoli, *Nat. Mater.*, 2009, **8**, 194; (*i*) O. Waldmann, T. C. Stamatatos, G. Christou, H. U. Güdel, I. Sheikin and H. Mutka, *Phys. Rev. Lett.*, 2009, **102**, 157202; (*j*) M. Affronte, *J. Mater. Chem.*, 2009, **19**, 1731; (*k*) T. Taguchi, W. Wernsdorfer, K. A. Abboud and G. Christou, *Inorg. Chem.*, 2010, **49**, 199; (*l*) S. N. Wang, L. Q. Kong, H. Yang, Z. T. He, Z. Jiang, D. C. Li, S. Y. Zheng, M. J. Niu, Y. Song and J. M. Dou, *Inorg. Chem.*, 2011, **50**, 2705; (*m*) G. P. Guedes, S. Soriano, N. M. Comerlato, N. L. Speziali, M. A. Novak and M. G. F. Vaz, *Inorg. Chem. Commun.*, 2013, **37**, 101; (*n*) F. J. Kettles, V. A. Milway, F. Tuna, R. Valiente, L. H. Thomas, W. Wernsdorfer, S. T. Ochsenbein and M. Murrie, *Inorg. Chem.*, 2014, **53**, 8970; (*o*) S. T. Liddle and J. van Slageren, *Chem. Soc. Rev.*, 2015, **44**, 6655.

2 (*a*) G. A. Craig and M. Murrie, *Chem. Soc. Rev.*, 2015, **44**, 2135; (*b*) S. Gómez-Coca, D. Aravena, R. Morales and E. Ruiz, *Coord. Chem. Rev.*, 2015, **289-290**, 379.

3 (*a*) D. Gatteschi, G. Christou and D. N. Hendrickson, *J. Am. Chem. Soc.*, 1993, **115**, 1804; (*b*) T. C. Stamatatos, V. Nastopoulos, A. J. Tasiopoulos, E. E. Moushi, W. Wernsdorfer, G. Christou and S. P. Perlepes, *Inorg. Chem.*, 2008, **47**, 10081; (*c*) J. Martínez-Lillo, A.-R. Tomsa, Y. Li, L.-M. Chamoreau, E. Cremades, E. Ruiz, A.-L. Barra, A. Proust, M. Verdaguer and P. Gouzerh, *Dalton Trans.*, 2012, **41**, 13668; (*d*) A. E. Thuijs, P. King, K. A. Abboud and G. Christou, *Inorg. Chem.*, 2015, **54**, 9127.

4 S. Gómez-Coca, E. Cremades, N. Aliaga-Alcalde and E. Ruiz, *Inorg. Chem.*, 2014, **53**, 676.

5 (*a*) E.-C. Yang, W. Wernsdorfer, S. Hill, R. S. Edwards, M. Nakano, S. Maccagnano, L. N. Zakharov, A. L. Rheingold, G. Christou and D. N. Hendrickson, *Polyhedron*, 2003, **22**, 1727; (*b*) M. Moragues-Cánovas, M. Helliwell, L. Ricard, É. Rivière, W. Wernsdorfer, E. Brechin and T. Mallah, *Eur. J. Inorg. Chem.*, 2004, **11**, 2219; (*c*) D. N. Hendrickson, E. C. Yang, R. M. Isidro, C. Kirman, J. Lawrence, R. S. Edwards, S. Hill, A. Yamaguchi, H. Ishimoto, W. Wernsdorfer, C. Ramsey, N. Dalal and M. M. Olmstead, *Polyhedron*, 2005, **24**, 2280; (*d*) E. C. Yang, W. Wernsdorfer, L. N. Zakharov, Y. Karaki, A. Yamaguchi, R. M. Isidro, G. Di Lu, S. A. Wilson, A. L. Rheingold, H. Ishimoto and D. N. Hendrickson, *Inorg. Chem.*, 2006, **45**, 529; (*e*) A. Ferguson, J. Lawrence, A. Parkin, J. Sanchez-Benitez, K. V. Kamenev, E. K. Brechin, W. Wernsdorfer, S. Hill and M. Murrie, *Dalton Trans.*, 2008, **37**, 6409; (*f*) F. Moro, F. Piga, I. Krivokapic, A. Burgess,

W. Lewis, J. McMaster and J. Van Slageren, *Inorg. Chim. Acta*, 2010, **363**, 4329; (*g*) S. Hameury, L. Kayser, R. Pattacini, G. Rogez, W. Wernsdorfer and P. Braunstein, *Dalton Trans.*, 2013, **42**, 5013.

6 (*a*) C. Cadiou, M. Murrie, C. Paulsen, V. Villar, W. Wernsdorfer and R. E. P. Winpenny, *Chem. Commun.*, 2001, **24**, 2666; (*b*) H. Andres, R. Basler, A. J. Blake, C. Cadiou, G. Chaboussant, C. M. Grant, G. Hans-Ulrich, M. Murrie, S. Parsons, C. Paulsen, F. Semadini, V. Villar, W. Wernsdorfer and R. E. P. Winpenny, *Chem. Eur. J.*, 2002, **8**, 4867; (*c*) S. T. Ochsenbein, M. Murrie, E. Rusanov, H. Stoeckli-Evans, C. Sekine and H. U. Güdel, *Inorg. Chem.*, 2002, **41**, 5133; (*d*) A. Bell, G. Aromí, S. J. Teat, W. Wernsdorfer and R. E. P. Winpenny, *Chem. Commun.*, 2005, **22**, 2808; (*e*) G. Aromí, S. Parsons, W. Wernsdorfer, E. K. Brechin and E. J. L. McInnes, *Chem. Commun.*, 2005, **40**, 5038; (*f*) E. Pardo, P. Burguete, R. Ruiz-García, M. Julve, D. Beltrán, Y. Journaux, P. Amorós and F. Lloret, *J. Mater. Chem.*, 2006, **16**, 2702; (*g*) Y.-R. Li, H.-Q. Liu, Y. Liu, S.-K. Su and Y.-P. Wang, *Chin. Phys. Lett.*, 2009, **26**, 077504; (*h*) R. T. W. Scott, L. F. Jones, I. S. Tidmarsh, B. Breeze, R. H. Laye, J. Wolowska, D. J. Stone, A. Collins, S. Parsons, W. Wernsdorfer, G. Aromí, E. J. L. McInnes and E. K. Brechin, *Chem. – Eur. J.*, 2009, **15**, 12389; (*i*) S. Petit, P. Neugebauer, G. Pilet, G. Chastanet, A. L. Barra, A. B. Antunes, W. Wernsdorfer and D. Luneau, *Inorg. Chem.*, 2012, **51**, 6645; (*j*) S. Hameury, L. Kayser, R. Pattacini, G. Rogez, W. Wernsdorfer and P. Braunstein, *Dalton Trans.*, 2013, **42**, 5013; (*k*) A. Ghisolfi, K. Y. Monakhov, R. Pattacini, P. Braunstein, X. López, C. de Graaf, M. Speldrich, J. van Leusen, H. Schilder and P. Kögerler, *Dalton Trans.*, 2014, **43**, 7847.

7 L. Ballester, E. Coronado, A. Guti, A. Mange, M. F. Perpifitin, E. Pinilla and T. Ricot, *Inorg. Chem.*, 1992, **31**, 2053.

8 (*a*) M. A. Halcrow, J. Sun, J. C. Huffman and G. Christou, *Inorg. Chem.*, 1995, **34**, 4167; (*b*) C. N. Complex, J. M. Clemente-juan, B. Donnadieu, J. Tuchagues and R. V. May, *Inorg. Chem.*, 2000, **4**, 5515; (*c*) A. Das, F. J. Klinke, S. Demeshko, S. Meyer, S. Dechert and F. Meyer, *Inorg. Chem.*, 2012, **51**, 8141; (*d*) S. Karmakar and S. Khanra, *CrystEngComm*, 2014, **16**, 2371; (*e*) P. S. Perlepe, A. A. Athanasopoulou, K. I. Alexopoulou, C. P. Raptopoulou, V. Psycharis, A. Escuer, S. P. Perlepes and T. C. Stamatatos, *Dalton Trans.*, 2014, **43**, 16605.

9 (*a*) Y. M. Li, J. J. Zhang, R. B. Fu, S. C. Xiang, T. L. Sheng, D. Q. Yuan, X. H. Huang and X. T. Wu, *Polyhedron*, 2006, **25**, 1618; (*b*) K. G. Alley, R. Bircher, H. U. Güdel, B. Moubaraki, K. S. Murray, B. F. Abrahams and C. Boskovic, *Polyhedron*, 2007, **26**, 369; (*c*) D. Mandal, C. S. Hong, H. C. Kim, H. K. Fun and D. Ray, *Polyhedron*, 2008, **27**, 2372; (*d*) Y. Xie, J. Ni, F. Zheng, Y. Cui, Q. Wang, S. W. Ng and W. Zhu, *Cryst. Growth Des.*, 2009, **9**, 118; (*e*) C. G. Efthymiou, C. Papatriantafyllopoulou, G. Aromi, S. J. Teat, G. Christou and S. P. Perlepes, *Polyhedron*, 2011, **30**, 3022; (*f*) R. Touzani, M. Haibach, A. J. Nawara-Hultzsch, S. El Kadiri, T. J. Emge and A. S. Goldman, *Polyhedron*, 2011, **30**, 2530; (*g*) G. M. Yu, L. Zhao, L. F. Zou, Y. N. Guo, G. F. Xu, Y. H. Li and J. Tang, *J. Chem. Crystallogr.*, 2011, **41**, 606; (*h*) J.-P. Costes, G. Novitchi, L. Vendier, G. Pilet and D. Luneau, *C. R. Chim.*, 2012, **15**, 849; (*i*) S. T. Meally, S. M. Taylor, E. K. Brechin, S. Piligkos and L. F. Jones, *Dalton Trans.*, 2013, **42**, 10315; (*j*) H. S. Wang and Y. Song, *Inorg. Chem. Commun.*, 2013, **35**, 86.

10 (*a*) S. Mukherjee, T. Weyhermüller, E. Bothe, K. Wieghardt and P. Chaudhuri, *Eur. J. Inorg. Chem.*, 2003, **5**, 863; (*b*) M. Koikawa, M. Ohba and T. Tokii, *Polyhedron*, 2005, **24**, 2257; (*c*) A. K. Ghosh, M. Shatruk, V. Bertolasi, K. Pramanik and D. Ray, *Inorg. Chem.*, 2013, **52**, 13894; (*d*) M. S. Jana, J. L. Priego, R. Jiménez-Aparicio and T. K. Mondal, *Spectrochim. Acta, Part A*, 2014, **133**, 714; (*e*) M. Pait, A. Bauzá, A. Frontera, E. Colacio and D. Ray, *Inorg. Chem.*, 2015, **54**, 4709.

11 K. S. Murray, in *Advances in Inorganic Chemistry*, ed. A. G. Sykes, Academic Press, 1995, vol. 43, p. 261.

12 G. Aromí, A. S. Batsanov, P. Christian, M. Helliwell, O. Roubeau, G. A. Timco and R. E. P. Winpenny, *Dalton Trans.*, 2003, **32**, 4466.

13 (*a*) P. King, R. Clerac, W. Wernsdorfer, C. E. Anson and A. K. Powell, *Dalton Trans.*, 2004, **977**, 2670; (*b*) C. G. Efthymiou, C. P. Raptopoulou, A. Terzis, R. Boča, M. Korabic, J. Mrozinski, S. P. Perlepes and E. G. Bakalbassis, *Eur. J. Inorg. Chem.*, 2006, **11**, 2236; (*c*) S. Banerjee, M. Nandy, S. Sen, S. Mandal, G. M. Rosair, A. M. Z. Slawin, C. J. Gómez García, J. M. Clemente-Juan, E. Zangrando, N. Guidolin and S. Mitra, *Dalton Trans.*, 2011, **40**, 1652; (*d*) S. Liu, S. Wang, F. Cao, H. Fu, D. Li and J. Dou, *RSC Adv.*, 2012, **2**, 1310; (*e*) V. Psycharis, B. A. Terzis and B. V. Tangoulis, *Aust. J. Chem.*, 2012, **65**, 1608.

14 (*a*) S. Hazra, R. Koner, P. Lemoine, E. Carolina Sañudo and S. Mohanta, *Eur. J. Inorg. Chem.*, 2009, **23**, 3458; (*b*) Y. Zhang, X. M. Zhang, T. F. Liu and W. G. Xu, *Transition Met. Chem.*, 2010, **35**, 851; (*c*) S. Shit, M. Nandy, G. Rosair, C. J. Gómez-García, J. J. B. Almenar and S. Mitra, *Polyhedron*, 2013, **61**, 73.

15 (*a*) A. Elmali, O. Atakol, I. Svoboda and H. Fuess, *Z. Kristallogr.*, 1992, **202**, 323; (*b*) A. Elmali, Y. Elerman, I. Svoboda and H. Fuess, *Acta Crystallogr., Sect. C: Cryst. Struct. Commun.*, 1993, **49**, 965; (*c*) A. Elmali, Y. Elerman, I. Svoboda, H. Fuess, K. Griesar and W. Haase, *Z. Naturforsch., B: Chem. Sci.*, 1994, **49**, 1239; (*d*) A. Elmali, Y. Elerman, I. Svoboda, H. Fuess, K. Griesar and W. Hasse, *Z. Naturforsch., B: Chem. Sci.*, 1994, **49**, 365; (*e*) A. Elmali, Y. Elerman, I. Svoboda and H. Fuess, *J. Mol. Struct.*, 2000, **516**, 43; (*f*) A. Elmali, Y. Elerman and I. Svoboda, *Z. Naturforsch., B: Chem. Sci.*, 2001, **56**, 897; (*g*) A. Elmali, Y. Elerman, C. T. Zeyrek and I. Svoboda, *Z. Naturforsch., B: Chem. Sci.*, 2003, **58**, 433; (*h*) K. C. Mondal, G. E. Kostakis, Y. Lan, W. Wernsdorfer, C. A. Anson and A. K. Powell, *Inorg. Chem.*, 2011, **50**, 11604; (*i*) I. Nemec, M. Machata, R. Herchel, R. Boča and Z. Trávníček, *Dalton Trans.*, 2012,

41, 14603; (*j*) P. Bag, J. Goura, V. Mereacre, G. Novitchi, A. K. Powell and V. Chandrasekhar, *Dalton Trans.*, 2014, **43**, 16366; (*k*) S. Saha, S. Pal, C. J. Gómez-García, J. M. Clemente-Juan, K. Harms and H. P. Nayek, *Polyhedron*, 2014, **74**, 1; (*l*) N. C. Anastasiadis, D. A. Kalofolias, A. Philippidis, S. Tzani, C. Raptopoulou, V. Psycharis, C. J. Milios, A. Escuer and S. P. Perlepes, *Dalton Trans.*, 2015, **44**, 10200; (*m*) W.-W. Kuang, C.-Y. Shao and P.-P. Yang, *J. Coord. Chem.*, 2015, **68**, 1412.

16 (*a*) J. W. Ran, S. Y. Zhang, B. Xu, Y. Xia, D. Guo, J. Y. Zhang and Y. Li, *Inorg. Chem. Commun.*, 2008, **11**, 73; (*b*) Q. Liang, R. Huang, X. Chen, Z. Li, X. Zhang and B. Sun, *Inorg. Chem. Commun.*, 2010, **13**, 1134; (*c*) S. Y. Zhang, W. Q. Chen, B. Hu, Y. M. Chen, W. Li and Y. Li, *Inorg. Chem. Commun.*, 2012, **16**, 74; (*d*) S. Nayak, G. Novitchi, S. Muche, D. Luneau and S. Dehnen, *Z. Anorg. Allg. Chem.*, 2012, **638**, 1127.

17 (*a*) C. Boskovic, E. Rusanov, H. Stoeckli-Evans and H. U. Güdel, *Inorg. Chem. Commun.*, 2002, **5**, 881; (*b*) A. Sieber, C. Boskovic, R. Bircher, O. Waldmann, S. T. Ochsenbein, G. Chaboussant, H. U. Güdel, N. Kirchner, J. van Slageren, W. Wernsdorfer, A. Neels, H. Stoeckli-Evans, S. Janssen, F. Juranyi and H. Mutka, *Inorg. Chem.*, 2005, **44**, 4315; (*c*) S.-S. Qian, Y. Zhao, M.-M. Zhen, C.-L. Zhang, Z.-L. You and H.-L. Zhu, *Transition Met. Chem.*, 2013, **38**, 63; (*d*) Z. Lu, T. Fan, W. Guo, J. Lu and C. Fan, *Inorg. Chim. Acta*, 2013, **400**, 191.

18 (*a*) G. Aromí, E. Bouwman, E. Burzurí, C. Carbonera, J. Krzystek, F. Luis, C. Schlegel, J. Van Slageren, S. Tanase and S. J. Teat, *Chem. – Eur. J.*, 2008, **14**, 11158; (*b*) C. G. Efthymiou, C. Papatriantafyllopoulou, N. I. Alexopoulou, C. P. Raptopoulou, R. Boča, J. Mrozinski, E. G. Bakalbassis and S. P. Perlepes, *Polyhedron*, 2009, **28**, 3373; (*c*) W.-H. Zhang, N. B. Sulaiman, P. X. S. Tio and T. S. A. Hor, *CrystEngComm*, 2011, **13**, 2915; (*d*) S.-H. Zhang, N. Li, C.-M. Ge, C. Feng and L.-F. Ma, *Dalton Trans.*, 2011, **40**, 3000; (*e*) J. P. Sun, L. C. Li and X. J. Zheng, *Inorg. Chem. Commun.*, 2011, **14**, 877; (*f*) A. B. Canaj, D. I. Tzimopoulos, A. Philippidis, G. E. Kostakis and C. J. Milios, *Inorg. Chem.*, 2012, **51**, 10461; (*g*) F. Habib, C. Cook, I. Korobkov and M. Murugesu, *Inorg. Chim. Acta*, 2012, **380**, 378; (*h*) C. Ding, C. Gao, S. Ng, B. Wang and Y. Xie, *Chem. – Eur. J.*, 2013, **19**, 9961; (*i*) S. H. Zhang, Y. D. Zhang, H. H. Zou, J. J. Guo, H. P. Li, Y. Song and H. Liang, *Inorg. Chim. Acta*, 2013, **396**, 119.

19 R. Herchel, I. Nemec, M. Machata and Z. Trávníček, *Inorg. Chem.*, 2015, **54**, 8625.

20 F. Neese, *WIREs Comput. Mol. Sci.*, 2012, **2**, 73.

21 (*a*) R. Herchel, L. Váhovská, I. Potočňák and Z. Trávníček, *Inorg. Chem.*, 2014, **53**, 5896; (*b*) B. Drahoš, R. Herchel and Z. Trávníček, *Inorg. Chem.*, 2015, **54**, 3352; (*c*) K. Matelková, R. Boča, Ľ. Dlháň, R. Herchel, J. Moncol, I. Svoboda and A. Mašlejová, *Polyhedron*, 2015, **95**, 45; (*d*) I. Nemec, R. Herchel, I. Svoboda, R. Boča and Z. Trávníček, *Dalton Trans.*, 2015, **44**, 9551.

22 R. Boča, Ľ. Dlháň, W. Haase, R. Herchel, A. Mašlejová and B. Papánková, *Chem. Phys. Lett.*, 2003, **373**, 402.

23 The standard deviations were calculated as $\sigma_i = (P_{ij}^{-1}\cdot S/(N - k))^{-1/2}$, where $P_{ij} = \sum(\delta\mu_n/\delta a_i\cdot\delta\mu_n/\delta a_j)$ and $S = \sum(\mu_n - \mu_n^{exp})^2$ with $n = 1$ to N; a_i and a_j are the fitted parameters, N is the number of the experimental points (sum of temperature and field dependent data), μ_n and μ_n^{exp} are the calculated and experimental effective magnetic moments for the given temperature and magnetic field.

24 (*a*) E. Liviotti, S. Carretta and G. Amoretti, *J. Chem. Phys.*, 2002, **117**, 3361; (*b*) S. Carretta, E. Liviotti, N. Magnani, P. Santini and G. Amoretti, *Phys. Rev. Lett.*, 2004, **92**, 207205.

25 A. Wilson, E.-C. Yang, D. N. Hendrickson and S. Hill, *Polyhedron*, 2007, **26**, 2065.

26 (*a*) J. Bartolomé, G. FIloti, V. Kuncser, G. Schinteie, V. Mereacre, C. E. Anson, A. K. Powell, D. Prodius and C. Turta, *Phys. Rev. B: Condens. Matter*, 2009, **80**, 014430; (*b*) R. Ishikawa, R. Miyamoto, H. Nojiri, B. K. Breedlove and M. Yamashita, *Inorg. Chem.*, 2013, **52**, 8300.

27 *CrysAlis software package, Version 1.171.33.52*, Agilent, Technologies, Yarnton, England.

28 G. M. Sheldrick, *Acta Crystallogr., Sect. C: Cryst. Struct. Commun.*, 2015, **71**, 3.

29 F. Neese, *WIREs Comput. Mol. Sci.*, 2012, **2**, 73.

30 (*a*) C. Lee, W. Yang and R. G. Parr, *Phys. Rev. B: Condens. Matter*, 1988, **37**, 785; (*b*) A. D. Becke, *J. Chem. Phys.*, 1993, **98**, 1372; (*c*) A. D. Becke, *J. Chem. Phys.*, 1993, **98**, 5648; (*d*) P. J. Stephens, F. J. Devlin, C. F. Chabalowski and M. J. Frisch, *J. Phys. Chem.*, 1994, **98**, 11623.

31 (*a*) E. Ruiz, J. Cano, S. Alvarez and P. Alemany, *J. Comput. Chem.*, 1999, **20**, 1391; (*b*) E. Ruiz, A. Rodríguez-Fortea, J. Cano, S. Alvarez and P. Alemany, *J. Comput. Chem.*, 2003, **24**, 982.

32 P. A. Malmqvist and B. O. Roos, *Chem. Phys. Lett.*, 1989, **155**, 189.

33 (*a*) C. Angeli, R. Cimiraglia, S. Evangelisti, T. Leininger and J. P. Malrieu, *J. Chem. Phys.*, 2001, **114**, 10252; (*b*) C. Angeli, R. Cimiraglia and J. P. Malrieu, *Chem. Phys. Lett.*, 2001, **350**, 297; (*c*) C. Angeli, R. Cimiraglia and J. P. Malrieu, *J. Chem. Phys.*, 2002, **117**, 9138; (*d*) C. Angeli, S. Borini, M. Cestari and R. Cimiraglia, *J. Chem. Phys.*, 2004, **121**, 4043; (*e*) C. Angeli, B. Bories, A. Cavallini and R. Cimiraglia, *J. Chem. Phys.*, 2006, **124**, 054108.

34 D. Ganyushin and F. Neese, *J. Chem. Phys.*, 2006, **125**, 024103.

35 F. Neese, *J. Chem. Phys.*, 2005, **122**, 034107.

36 R. Maurice, R. Bastardis, C. Graaf, N. Suaud, T. Mallah and N. Guihéry, *J. Chem. Theory Comput.*, 2009, **5**, 2977.

37 (*a*) A. Schafer, H. Horn and R. Ahlrichs, *J. Chem. Phys.*, 1992, **97**, 2571; (*b*) A. Schafer, C. Huber and R. Ahlrichs, *J. Chem. Phys.*, 1994, **100**, 5829; (*c*) F. Weigend and R. Ahlrichs, *Phys. Chem. Chem. Phys.*, 2005, **7**, 3297.

38 (*a*) F. Neese, F. Wennmohs, A. Hansen and U. Becker, *Chem. Phys.*, 2009, **356**, 98; (*b*) R. Izsak and F. Neese, *J. Chem. Phys.*, 2011, **135**, 144105.

